www.springer.com/41230
https://doi.org/10.1007/s41230-025-4287-7

Effect of quenching, lamellarizing, and tempering heat treatment on cryogenic toughness of ZG14Ni3Cr1MoV steel

Chang-fu Li[1, 2], Yun-bao Gao[1, 2], Bao-zhi Li[1, 2], Ling Zhao[1, 2], Yu Wang[1, 2], Hai-jun Zhang[2], Qiu Du[2], and *Zeng-rui Wang[1, 2]

1. State Key Laboratory of Advanced Casting Technologies, Shenyang 110022, China

2. Shenyang Research Institute of Foundry Co., Ltd. CAM, Shenyang 110022, China

Abstract: The present work aims to investigate the effects of quenching, lamellarizing, and tempering (QLT) heat treatment on the microstructure and mechanical properties of ZG14Ni3Cr1MoV high-strength low-alloy (HSLA) steel by comparing with traditional quenching and tempering (QT) heat treatment. Following the various QLT heat treatments, a dual-phase microstructure consisting of "soft" ferrite and "hard" tempered bainite is obtained, exhibiting significantly refined grain sizes (38.87 to 46.51 μm for QLT samples) compared to QT samples (64.93 μm). As the lamellar quenching temperature increases from 750 °C to 810 °C, the yield strength and tensile strength of the QLT samples increase, although they remain lower than those of the QT samples. Conversely, elongation at fracture, reduction of area, and the product of strength and elongation synergy decrease, yet consistently exceed QT levels. Notably, the QLT samples demonstrate superior cryogenic impact toughness within the range of −80 °C to −120 °C, achieving optimal values after 910 °C quenching + 780 °C lamellar quenching + 670 °C tempering: 215.97 J at −80 °C, 207.80 J at −100 °C, and 183.17 J at −120 °C. This exceptional cryogenic toughness is attributed to two key mechanisms in the dual-phase microstructure: (i) a low dislocation density that suppresses crack initiation, and (ii) crack-tip passivation by soft ferrite, coupled with crack deflection and hindrance at high-angle grain boundaries (HAGBs). The results establish QLT as a viable method for enhancing cryogenic toughness in ZG14Ni3Cr1MoV HSLA steels.

Keywords: high-strength low-alloy steels; ZG14Ni3Cr1MoV steel; quenching; lamellarizing; tempering; cryogenic toughness; microstructure

CLC numbers: TG142.33 **Document code:** A **Article ID:** 1672-6421(2025)04-407-10

1 Introduction

High-strength low-alloy (HSLA) steels, known for their high strength, excellent toughness, good weldability, lower yield ratio, and excellent corrosion resistance, are widely utilized in various fields, including shipbuilding, automotive manufacturing, construction, bridge engineering, and offshore applications[1]. Currently, the carbon content of HSLA steels, such as the HY series from the United States, the NS series from Japan, and the АБ series from Russia, typically exceeds 0.1%. Additionally, elements such as nickel (Ni), chromium (Cr), molybdenum (Mo), and vanadium (V) are added to enhance hardenability and strength[2, 3]. Traditionally, HSLA steels are typically subjected to quenching (Q) and tempering (T) heat treatment to develop tempered sorbite microstructures, achieving a favorable balance of high strength and toughness. Although the quenching and tempering process has advantages in improving mechanical properties, the cryogenic toughness of HSLA steels exhibits a limited margin, which poses a significant challenge to industrial applications requiring high low-temperature toughness[4].

To address the aforementioned issue, a special heat treatment process consisted of quenching, lamellarizing, and tempering (QLT) has been introduced to replace the conventional quenching and tempering (QT) heat treatment[5, 6]. In general, the QLT process involves an initial quenching followed by reheating to the dual-phase

***Zeng-rui Wang**

Male, born in 1984, Ph. D., Senior Engineer. His research interests primarily focus on shape control of large and complex thin-walled cast steel (iron) parts and residual stress control throughout the entire manufacturing cycle.

E-mail: wangzr_srif@foxmail.com

Received: 2024-12-20; Revised: 2025-04-08; Accepted: 2025-04-21

region (α+γ) and then a second quenching, resulting in a dual-phase microstructure that consists of "hard" martensitic or bainitic phases. After tempering, a dual-phase microstructure consisting of tempered sorbite or tempered bainite combined with ferrite is obtained. This microstructure demonstrates satisfactory strength and excellent cryogenic toughness, along with overall favorable mechanical properties. The results indicate that the austenite grain size and martensite lath width of the QLT samples are refined, leading to a reduction in the ductile-brittle transition temperature (DBTT) compared to the QT samples[7]. Shafiei et al.[8] found that the retained austenite content in the QLT sample was lower than that in the QT sample, which resulted in slightly lower yield and tensile strengths, but a higher elongation due to the refinement of the microstructure. Yu et al.[9] performed QLT heat treatment on HSLA steels and achieved a heterogeneous microstructure composed of "soft" ferrite and "hard" tempered martensite, which resulted in high impact toughness. This excellent toughness was attributed to the decreased hardness difference between the soft and hard phases, as well as the high density of high-angle grain boundaries. Wang et al.[10] concluded that the HSLA steels treated with the QLT heat treatment could lead to a refinement of grain size and the formation of a dual-phase microstructure. This, in turn, was found to enhance cryogenic toughness. In summary, QLT heat treatment is an effective method for enhancing the cryogenic toughness of HSLA steels[7-10].

Some researchers compared the effects of QT and QLT heat treatments on the cryogenic toughness of ZG14Ni3Cr1MoV high-strength low-alloy steel[10], but the mechanisms by which QLT heat treatment improves the cryogenic toughness of this material have not been analyzed in detail. Therefore, in this study, characterization techniques such as OM, SEM, EDS, XRD, and EBSD, along with experiments including room temperature tensile tests and cryogenic impact tests at −80 °C, −100 °C, and −120 °C were utilized to systematically elucidate the toughening mechanisms of ZG14Ni3Cr1MoV high-strength low-alloy steel following QLT heat treatment. The objective is to enhance the cryogenic toughness of the steel and provide both theoretical support and technical solutions for optimizing heat treatment processes and improving product performances.

2 Experimental procedure

The chemical compositions of the studied ZG14Ni3Cr1MoV steel are as follows (in weight percent, wt.%): C 0.14, Si 0.23, Mn 0.42, and Ni+Cr+Mo+V is 4.09, balanced with Fe. After melting in an electric arc furnace and an AOD furnace, the molten steel was poured into sand molds to create test blocks with dimensions of 250 mm×170 mm×150 mm. All samples were taken from the mid-thickness (1/2 thickness) of the test blocks for subsequent heat treatment experiments. The studied steel underwent two distinct heat treatment processes, QLT and QT, of which the QT heat treatment served as a comparative benchmark. Prior to these two heat treatments, the studied steel underwent dehydrogenation annealing, diffusion annealing, and normalizing to reduce hydrogen atomic content, homogenize the chemical composition, and refine the grains for the subsequent quenching heat treatment.

The starting temperature of the ferrite-to-austenite transformation (A_{c1}) and the finishing temperature of the ferrite-to-austenite transformation (A_{c3}) of the studied steel were determined using differential scanning calorimetry (DSC). The experimental device utilized was an STA449F3 1693 synchronous thermal analyzer. The temperature was elevated to 950 °C, and the heating rates were established at 5 °C·min^{-1}, 10 °C·min^{-1}, 15 °C·min^{-1}, and 20 °C·min^{-1}.

The heat treatment experiments were conducted in a box-type resistance furnace. After austenitizing at 910 °C, all samples were quenched in water to obtain a fully bainitic microstructure and then divided into two groups. One group (QT samples) was tempered at 670 °C, while the other group (QLT samples) was subjected to lamellar quenching at temperatures of A_{c1}+20 °C, 50 °C, and 80 °C, respectively, holding for 225 min, followed by tempering at 670 °C, and holding for 375 min.

After heat treatment, the samples were machined into tensile samples with dimensions of Φ10 mm×124 mm and Charpy impact samples measuring 10 mm×10 mm×55 mm, featuring a 45° V-notch. The room-temperature tensile tests were conducted using a DDL300 electronic universal testing machine at a strain rate of 0.00025 s^{-1}. The Charpy impact tests were carried out on a NI 300AC digital impact testing machine, at temperatures of −80 °C, −100 °C, and −120 °C. Nitrogen gas was used as the temperature control medium. The microstructures of the samples at various heat treatment stages were observed and photographed using a JEISS Axio Vert. A1 inverted universal materials microscope, with a 4% nitric alcohol solution employed as the etchant. The grain size of the studied steel after tempering was measured using the Image-Pro Plus software. After conducting the Charpy impact tests, the fracture surfaces were immersed in alcohol, and ultrasonic cleaning was performed for 3 min to remove surface contaminants. The samples were then dried using a blow dryer and examined for fracture morphology with an EVO MA25 scanning electron microscope (SEM). The composition of inclusions at the impact fracture was analyzed using the energy dispersive spectroscopy (EDS) attached to the SEM equipment.

For metallographic preparation, the sample surfaces were polished and subsequently electro-polished. The electro-polishing solution was prepared with 90% anhydrous ethanol and 10% perchloric acid (by volume). A voltage of 20 V and a current of 1 A were then applied to the solution for a duration of 15 s. The electro-polished samples were then used for crystallographic orientation analysis using SEM. The accelerating voltage of the SEM was set to 20 kV, the working distance was adjusted to a tilt angle of 70°, and the step size was 0.5 μm. EBSD data were processed using the Channel5 software. The phase constitution was analyzed using a Bruker D8 Focus X-ray diffractometer (XRD) by collecting diffraction peaks from crystal planes.

3 Results

3.1 Differential scanning calorimetry experiment

The DSC curves of the studied steel are presented in Fig. 1. The curves indicate that the A_{c1} temperature of the studied steel is determined to be 730 °C, while the A_{c3} temperature is found to be 830 °C. Consequently, temperatures of 750 °C, 780 °C, and 810 °C were selected as the lamellar quenching temperatures.

3.2 Microstructure characterization

From the XRD spectra presented in Fig. 2, it is evident that the XRD patterns of both the QT and QLT samples are predominantly characterized by peaks corresponding to (110)α, (200)α, and (211)α. The phase constitution of the samples following both heat treatments exhibits a body-centered cubic (BCC) structure, with no residual austenite being detected.

The microstructures of the samples subjected to various heat treatment conditions are illustrated in Fig. 3. The Q sample, which was quenched at 910 °C, exhibits a typical lath bainite (LB) microstructure, as shown in Fig. 3(a). The metallographic image of the Q sample after 670 °C tempering (QT) is shown in Fig. 3(b). After tempering, most of the lath boundaries become ambiguous owing to the recovery of the bainitic

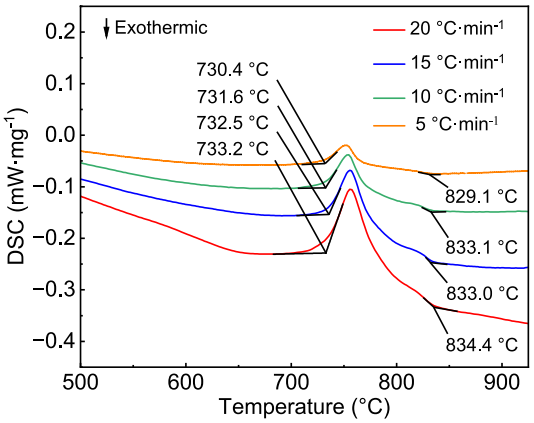

Fig. 1: DSC curves of experimental steels

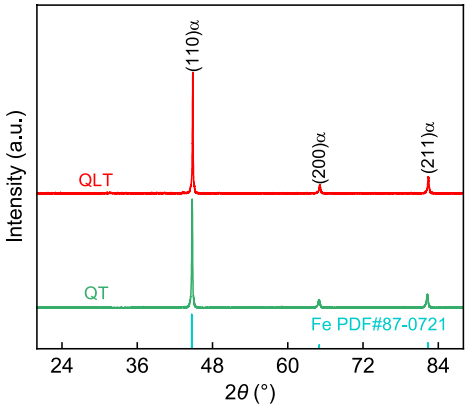

Fig. 2: XRD patterns of samples after various heat treatments

microstructure. A significant amount of dispersed second-phase particles is observed in the tempered bainitic microstructure, and their grain size is greater than that prior to tempering.

Figures 3(c), (e), and (g) present the metallographic images of the samples after lamellar quenching at 750 °C, 780 °C, and 810 °C (labeled as QL-1, QL-2, and QL-3), respectively. After lamellar quenching, the samples exhibit a dual-phase microstructure composed of block ferrite (F) and lath bainite (LB). It is reasonable to speculate that the variation in the microstructures of the three lamellar samples is attributed to the differences in bainite content. When the steel is maintained at 750 °C, a temperature near the A_{c1} point, incomplete diffusion of carbon and alloying elements hinders the nucleation and growth of austenite. As a result, the amount of austenite formed at this temperature is limited, which negatively affects the bainite content in the microstructure after lamellar quenching. As the lamellar quenching temperature increases, the bainite content gradually rises. Finally, after laminar quenching at 810 °C, the bainite content in the microstructure of the QL-3 sample reaches its peak. Figures 3(d), (f), and (h) reveal the metallographic structures of the QL samples after tempering at 670 °C. Following tempering, the lath bainite structure undergoes recovery, characterized by the merging of adjacent bainite

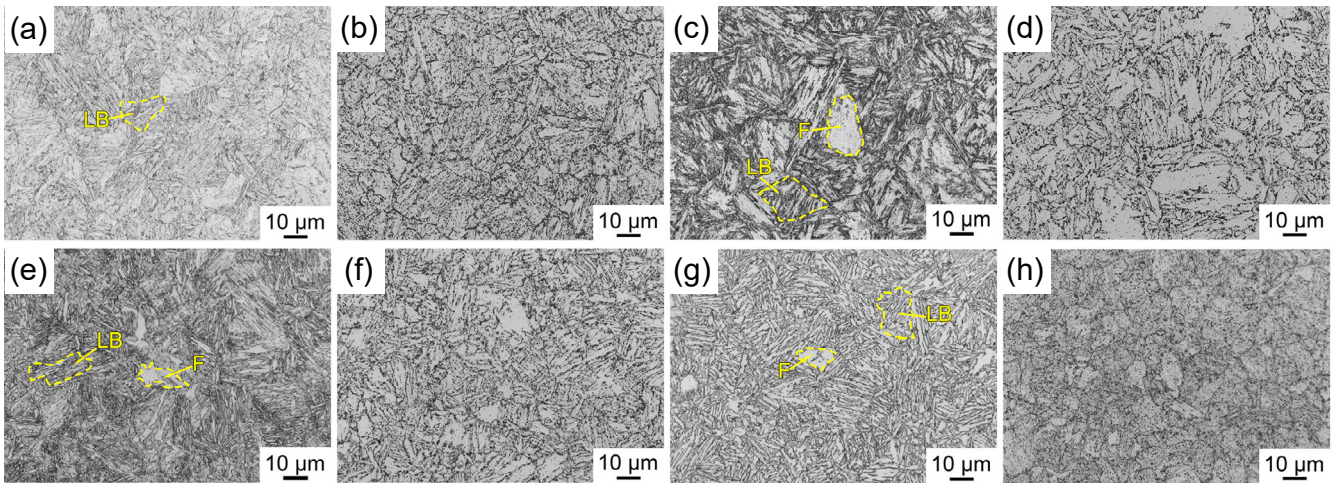

Fig. 3: Microstructures of steels following various heat treatment conditions: (a) Q; (b) QT; (c) QL-1; (d) QLT-1; (e) QL-2; (f) QLT-2; (g) QL-3; (h) QLT-3

laths into a broader lath structure. This process also leads to the precipitation of black, point-like carbides within the laths, along grain boundaries, and at dislocations.

Figure 4 illustrates the grain size statistics of primary austenite in the experimental steel following various heat treatments. In Fig. 4(a), it can be seen that the average grain size of the QT sample is 64.93 μm, with 50% of the total grains is finer than 55.95 μm, while 90% of the total grains has a grain size smaller than 99.10 μm. Figures 4(b), (c), and (d) present the grain size statistics of samples subjected to different lamellar quenching temperatures and after tempering. During the heating stage of lamellar quenching, defects such as dislocations and vacancies would be generated during the transformation of lath bainite to austenite, which increases the stored energy of austenite[11]. In the subsequent cooling process, this accumulated stored energy enhances the nucleation rate, resulting in refined grain sizes. At a lamellar quenching temperature of 750 °C, which is close to the A_{c1} point, the driving force for the austenite phase transformation is low. This results in a decreased austenite nucleation rate, adversely affecting the cooling process and leading to a large grain size of approximately 45.62 μm. However, as the lamellar quenching temperature increases to 780 °C, the driving force for the austenite phase transformation rises, which in turn increases the austenite nucleation rate and reduces the grain size to 38.87 μm. However, as the lamellar quenching temperature continues to rise to 810 °C, the pinning effect of undissolved carbides on the grain boundaries weakens, causing the grain size of the QLT sample to increase again to 46.51 μm. However, the grain size of all the OLT samples is obviously finer than that of the QT sample. In particular, the average grain size of the QLT-2 sample is 38.87 μm, with 50% of the grains measuring less than 32.27 μm and the majority of the grains finer than 56.52 μm. Namely, the QLT-2 sample exhibits the finest grain size among all QLT samples. Based on previous research works[12, 13], it is known that grain refinement can alter the crack path, hinder crack propagation, and significantly enhance the cryogenic toughness of the materials. Therefore, grain refinement is likely one of the factors contributing to the superior cryogenic toughness observed in QLT samples.

From the phase volume fraction curve demonstrated in Fig. 5, it is evident that as the lamellar quenching temperature increases from 750 °C to 810 °C, the bainite content within the QLT sample steadily increases, reaching values of 28.6%, 50.8%, and 69.8%, respectively. In contrast, the ferrite content gradually decreases, reaching 71.4%, 49.2%, and 30.2%, respectively. At 750 °C, which is close to the A_{c1} point, carbon and alloying elements lack sufficient time for complete diffusion, thereby delaying the nucleation and growth of austenite. Consequently, a dual-phase structure consisting of ferrite and a limited amount of new bainite forms. As the lamellar quenching temperature increases to beyond 750 °C, the proportion of bainite within this dual-phase structure gradually increases. At 810 °C, the microstructure of the QLT sample attains a tempered bainite content of 69.8%.

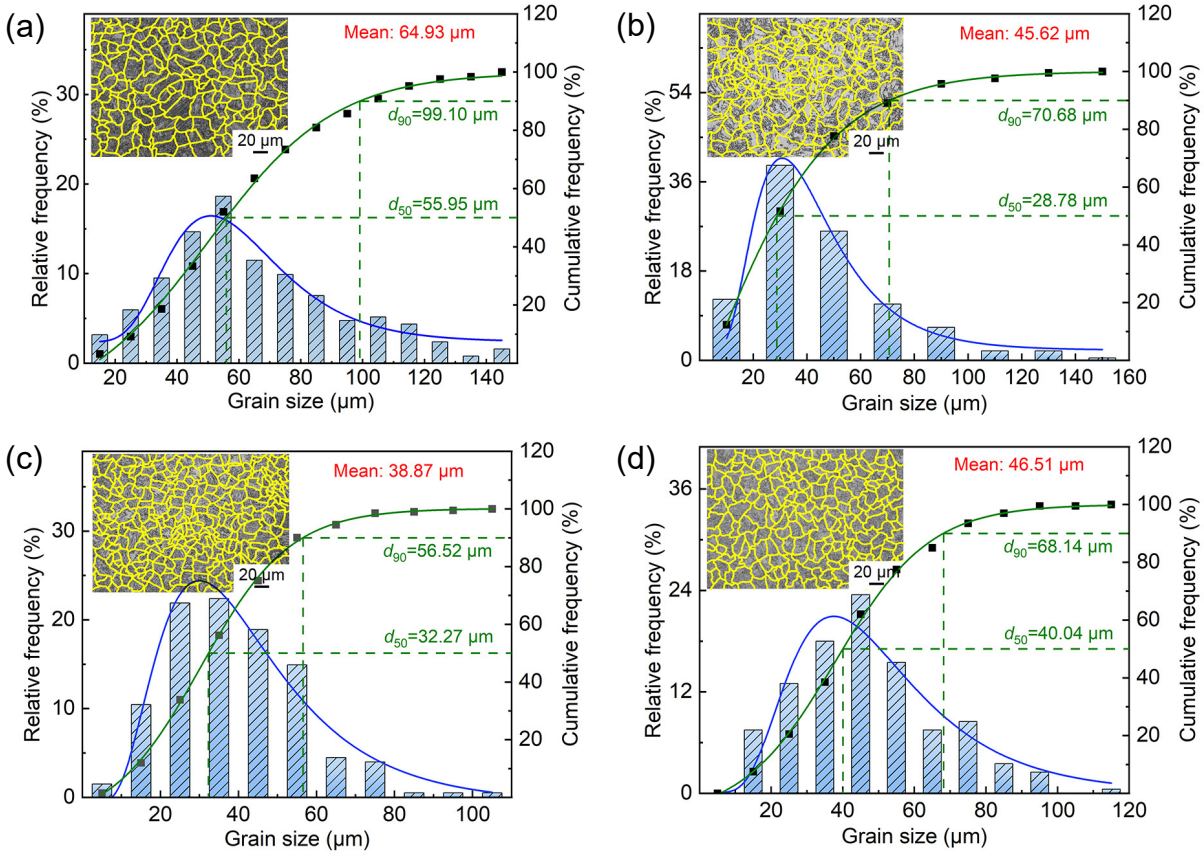

Fig. 4: Grain size statistics of samples with various heat treatments: (a) QT; (b) QLT-1; (c) QLT-2; (d) QLT-3

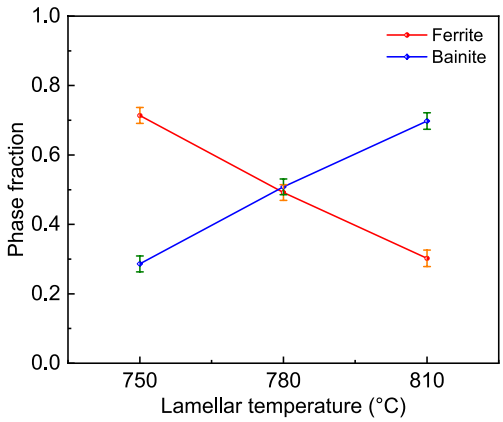

Fig. 5: Statistics of phase volume fraction in QLT samples

3.3 Mechanical properties

The mechanical properties of the studied steel after QT and QLT process, including ultimate tensile strength (UTS), yield strength (YS), elongation at fracture (A), reduction of area (Z), and the product of strength and elongation (PSE) are presented in Fig. 6 and Table 1. The strength and plasticity of the studied steel change significantly after QT and QLT processes. The UTS and YS of the QT samples are 780.5 MPa and 711 MPa, respectively, both of which are higher than those of the QLT samples. However, their values of A (18.75%), Z (70.50%), and PSE (14.63 GPa·%) are lower than the QLT samples. These results indicate that the studied steel exhibits poor plasticity after QT process. For the QLT samples, as the lamellar quenching temperature increases from 750 °C to 810 °C, the UTS gradually increases from 632.50 MPa to 725.50 MPa, representing an increase of 14.70%. Similarly, the YS increases from 494.00 MPa to 638.50 MPa, reflecting a rise of 29.30%. In contrast, A, Z, and PSE exhibit a falling trend, decreasing from 27.75%, 73.50%, and 17.55 GPa·% to 20.50%, 71.00%, and 14.87 GPa·%, a decrease of 26.13%, 3.40%, and 15.27%, respectively. As the lamellar quenching temperature increases, the strength is significantly improved, while plasticity tends to decline. Nevertheless, the plasticity of the QLT samples remain superior to those of the QT samples.

Based on the QT and QLT processes, the impact absorption energy of the studied steel at various lamellar quenching

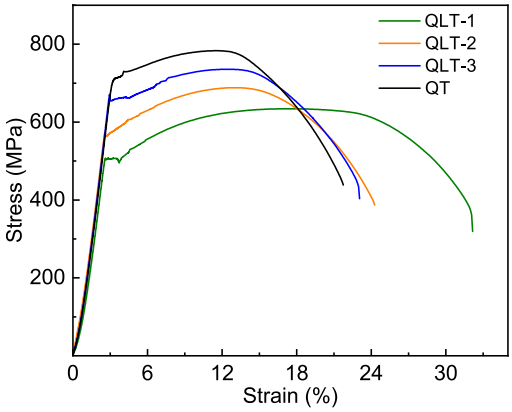

Fig. 6: Stress-strain curves of samples with various heat treatments

Table 1: Mechanical properties of various heat treatment samples

Samples	Heat treatment temperature (°C)	YS (MPa)	UTS (MPa)	A (%)	Z (%)	PSE (GPa·%)
QT	910+670	711.00	780.50	18.75	70.50	14.63
QLT-1	910+750+670	494.00	632.50	27.75	73.50	17.55
QLT-2	910+780+670	556.50	679.00	23.50	73.00	15.96
QLT-3	910+810+670	638.50	725.50	20.50	71.00	14.87

temperatures is illustrated in Fig. 7. Within the temperature range of −80 °C to −120 °C, the QLT samples demonstrate remarkably higher impact absorption energy compared to the QT samples. The QLT-2 process leads to the most excellent cryogenic toughness values of 215.97 J at −80 °C, 207.80 J at −100 °C, and 183.17 J at −120 °C, achieved through lamellar quenching at 780 °C. In contrast, the impact absorption energy of the QT samples is 157.93 J at −80 °C, 60.90 J at −100 °C, and 36.80 J at −120 °C. This suggests that the QLT process significantly enhances the cryogenic toughness of the studied steel.

In conclusion, the studied steel demonstrates a reduction in strength following the QLT process. However, there is a remarkable enhancement in toughness. Furthermore, cryogenic toughness exhibits substantial improvements, with the QLT-2 heat treatment producing the most notable advancements.

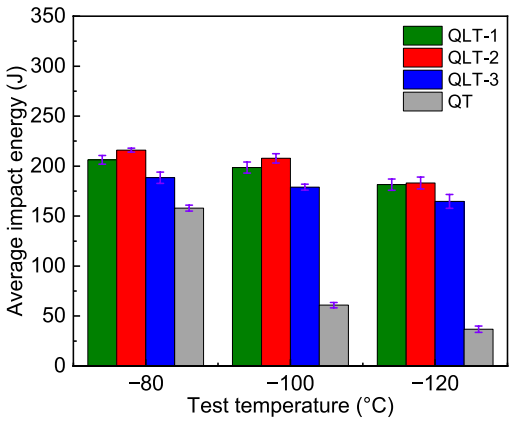

Fig. 7: Impact absorption energy curves at various lamellar quenching temperatures

3.4 Impact fracture morphology

The SEM images and EDS spectrum of the impact fracture morphology of the samples following various heat treatments, tested at −100 °C, are shown in Fig. 8, where Fig. 8(e) shows the EDS point position in the QT sample. Typical features of brittle fracture are observed on the fracture surface of the QT sample, as shown in Fig. 8(a), which are characterized by a river pattern consisting of flat cleavage planes. The EDS spectrum obtained at the position of the red five-pointed star in Fig. 8(e) suggests that these white elliptical particles are likely a mixture of oxide (Al_2O_3) and sulfide (MnS). It should be noted that the position shown in Fig. 8(e) is near the surface of the QT

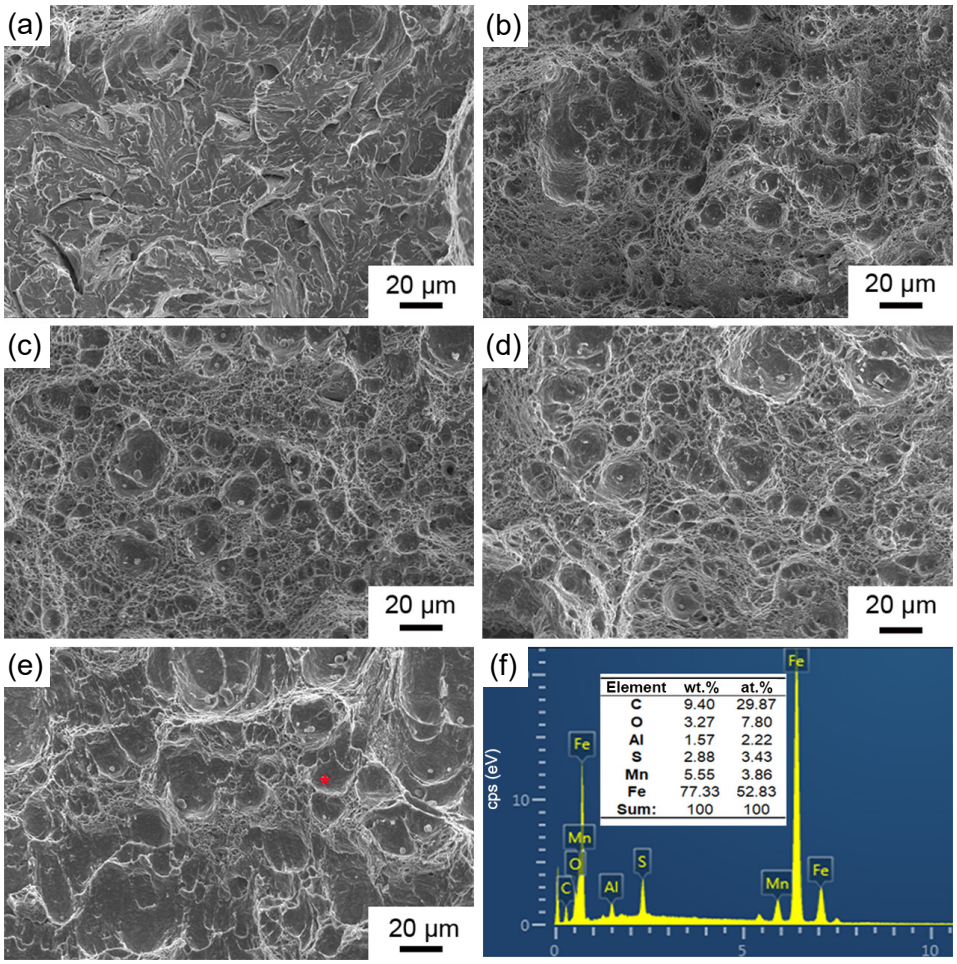

Fig. 8: Morphologies of impact fracture samples following various heat treatment conditions at –100 °C: (a) QT; (b) QLT-1; (c) QLT-2; (d) QLT-3; (e) EDS point position in QT sample; (f) EDS spectrum

sample; this image is provided solely to indicate the location of the EDS measurement point. A small amount of plastic deformation occurs near the surface of the QT sample at the onset of the impact test, forming a series of shallow, small dimples; however, this does not represent the fracture condition of the QT sample. Figures 8(b), (c), and (d) depict the impact fracture morphologies after the QLT process. The fracture surfaces display typical characteristics of ductile fracture, featuring deep, unevenly sized dimples. These dimples serve as the nucleation sites for microvoids during ductile fracture, indicating that substantial plastic deformation takes place, thereby alleviating the stress at the main crack tip. In addition, different sizes of dimples contribute to a greater absorption of impact energy. Therefore, the cryogenic toughness of the QLT samples is enhanced. It can be inferred that the energy absorbed by the QLT samples during the crack propagation stage will exceed that of the QT sample.

During impact plastic deformation, the physical and chemical differences between the inclusions and the matrix disrupt the continuity and homogeneity of the steel, leading to local stress concentrations and the formation of microcracks[14]. As deformation progresses, microcracks propagate along the inclusions and develop into voids. The coalescence of adjacent voids ultimately results in fracture.

4 Discussion

4.1 Effect of microstructure on cryogenic toughness

With the same alloy composition, the cryogenic toughness of the material is influenced by the processing technology, grain size, microstructure, and retained austenite content[13-16]. As mentioned above, no austenite is found in the XRD spectra of QT and QLT samples. In other words, transformation-induced plasticity (TRIP) is unlikely to occur[17]. Therefore, in the present work, improving the cryogenic toughness of the test steel is mainly associated with the processing technology, grain size, and microstructure.

It is well known that the toughness of a material is related to the nucleation and propagation of cracks[18]. The Yoffee diagram[19] illustrates the relative probabilities of ductile versus brittle fracture occurring at the crack tip, as shown in Fig. 9. Under the influence of applied stress, the stress δ at the crack tip can be categorized into two scenarios: If δ is greater than the effective yield stress δ_Y but less than the brittle fracture stress δ_F ($\delta_Y<\delta<\delta_F$), ductile deformation is more likely to occur than brittle fracture. Conversely, if δ is less than δ_Y or greater than δ_F ($\delta_F<\delta<\delta_Y$), a brittle fracture is expected to occur.

Therefore, on the basis of the Yoffee diagram, two methods

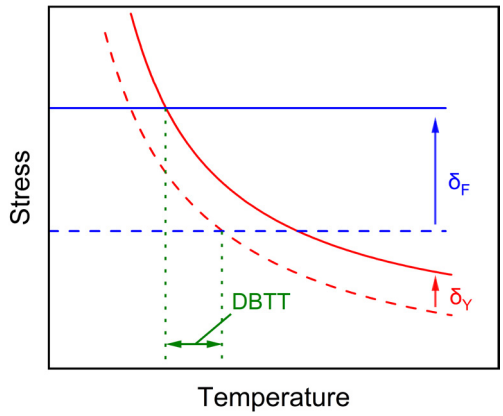

Fig. 9: Yoffee diagram showing ductile-brittle transition temperature (DBTT)[20]

are identified to suppress the ductile-brittle transition of materials: increasing the brittle fracture stress (δ_F) or decreasing the effective yield stress (δ_Y). Both δ_Y and δ_F can be expressed using the Hall-Petch equation and its variations[20], as demonstrated in the following equations:

$$\delta_Y = \delta_0 + K_Y d^{-1/2} \quad (1)$$

$$\delta_F = K_F d^{-1/2} \quad (2)$$

where, K_Y and K_F represent the Hall-Petch slope and the fracture slope, respectively, and d is the grain size. According to Eqs. (1) and (2), it can be concluded that both δ_Y and δ_F are linearly related to $d^{-1/2}$ and increase with a decrease in the grain size. However, studies have shown that grain size refinement has a greater effect on δ_F, making it larger than δ_Y[21, 22]. In the present work, the grain size is refined following QLT heat treatment, which increases the δ_F and facilitates plastic deformation, thereby enhancing the cryogenic toughness of the studied steel. At the same time, the presence of "soft" ferrite in the dual-phase microstructure can relax the stress field at the crack tip, reduce the probability of crack initiation, and passivate the crack. This significantly increases resistance to crack propagation and improves cryogenic toughness.

To better understand the effect of grain refinement on cryogenic toughness, the band contrast (BC) map and misorientation distribution statistics were performed, as presented in Fig. 10. Grain boundaries can be categorized into two types based on the misorientation angle (θ): those represented by yellow lines (where $2°<\theta<15°$) and those marked by red lines (where $\theta \geq 15°$). The microstructure of the QT sample [Fig. 10(a)] consists of lath structures, whereas the microstructure of the QLT samples [Figs. 10(c), (e), and (g)] is characterized by blocky or lath-shaped structures, which aligns with the metallographic results. Grain boundaries with misorientation angles greater than 15° are typically classified as high-angle grain boundaries (HAGBs)[23]. Some reports[24] pointed out that the interface between ferrite and bainite after lamellar quenching is characterized by HAGBs. As shown in Fig. 10, a dual-phase microstructure consisting of ferrite and tempered bainite is formed following the QLT process, and the density of HAGBs is noticeably higher compared to the 37% observed in the QT sample, which aligns with findings from previous studies. When the lamellar quenching temperature rises from 750 °C to 810 °C, the density of HAGBs in the QLT sample initially increases and then decreases. The HAGBs percentages are 49%, 51%, and 44%, respectively.

HAGBs are effective in preventing the formation and propagation of cracks, whereas low-angle grain boundaries (LAGBs) have minimal effect on these processes. HAGBs increase the energy loss of cracks by impeding their propagation and deflecting their direction, thereby contributing to the enhancement of cryogenic toughness[25]. The higher density of HAGBs observed after QLT process, in comparison to QT process, is closely related to the refinement of the microstructure.

A higher dislocation density has a certain inhibitory effect on the further propagation of dislocations[26]. According to Griffith's microcrack theory, the critical fracture strength σ_c of materials subjected to plane strain can be expressed as follows[27]:

$$\sigma_c = \left[\frac{E(2\gamma_s + \gamma_p)}{(1-\nu^2)\pi a_c}\right]^{1/2} \quad (3)$$

where, E represents Young's modulus, ν denotes Poisson's ratio, a_c refers to the critical crack size (which is the length of the surface crack or half the length of the central crack), γ_s is the specific surface energy of the material, and γ_p indicates the plastic work required to form a crack per unit area, which is positively correlated with the density of movable dislocations. During the plastic deformation process, a higher dislocation density facilitates interactions between dislocations. This interaction hinders the slip of dislocations, decreasing in the number of movable dislocations. Therefore, local stress concentrations are more likely to occur, reducing the plastic deformation work γ_p and increasing the probability of crack initiation and propagation.

The Kernel average misorientation (KAM) map, generated from the analysis of the EBSD data and illustrated in Fig. 11, serves as a tool for characterizing the distribution of local dislocation density. As shown in Figs. 11(a) to (d), the QLT samples exhibit a sparser dislocation distribution compared to the QT samples. Furthermore, as demonstrated in Fig. 11(e), the KAM distribution of the QLT samples shifts toward the lower left area compared with QT samples. Notably, the KAM distribution of the QLT-2 sample is positioned closest to the left side, indicating that it has the lowest dislocation density among the QLT samples. These observations suggest that compared to QT heat treatment, QLT heat treatment is more effective in reducing dislocation density while potentially increasing the number of mobile dislocations, resulting in improved coordination of deformation between ferrite and tempered bainite. This indicates that when ferrite undergoes substantial plastic deformation, tempered bainite also experiences a certain degree of yielding, which reduces the probability of microcracks forming at the interface between the two phases. Additionally, ferrite can passivate the crack tip and effectively hinder crack propagation. Hence, the

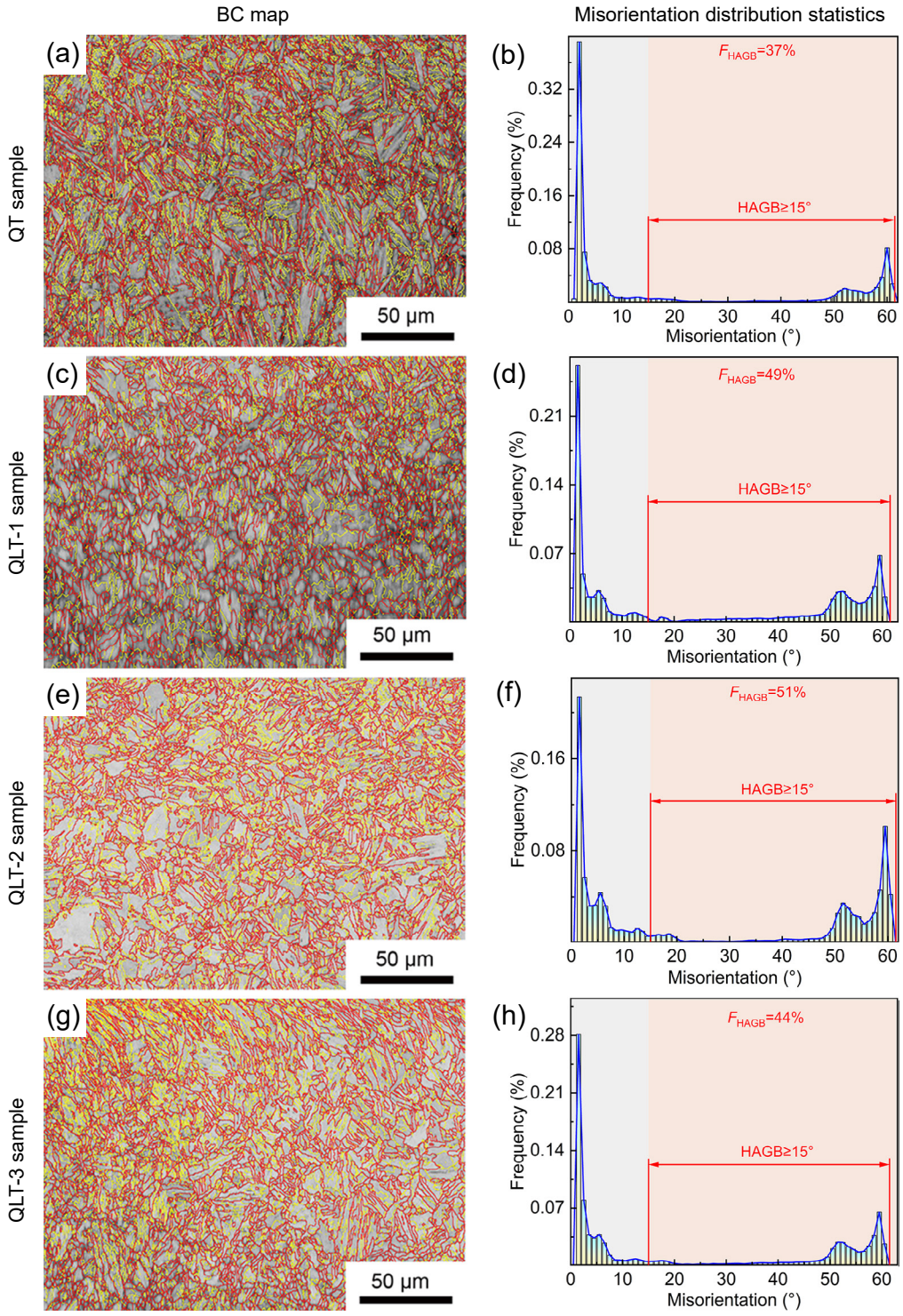

Fig. 10: BC map (a, c, e, g) and misorientation distribution statistics (b, d, f, h) of samples under various heat treatment conditions

lower dislocation density in the dual-phase microstructure, along with the blunting of the crack tip by the softer ferrite, contributes to the improved cryogenic toughness of the QLT sample.

Based on the aforementioned analysis, the rationale for the improvement of cryogenic toughness through the QLT process can be attributed to the decrease of dislocation density within the resulting dual-phase microstructure, as well as the passivation of crack tips by ferrite, and the increase in the density of HAGBs.

4.2 Grain size refinement

Schematic diagram of the structural transformation is illustrated in Fig. 12. After heating the studied steel to the austenite (γ) phase region and subsequently water cooling, a full lath bainite (LB) structure is obtained [Fig. 12(b)]. During the re-heating process to the (γ+α) dual-phase region, new austenite (New-A) can nucleate either at the primary austenite (PA) grain boundaries or at the boundaries of the LB lath [Fig. 12(c)]. At the same time, the complete diffusion of carbon and alloying elements in the untransformed LB results in its

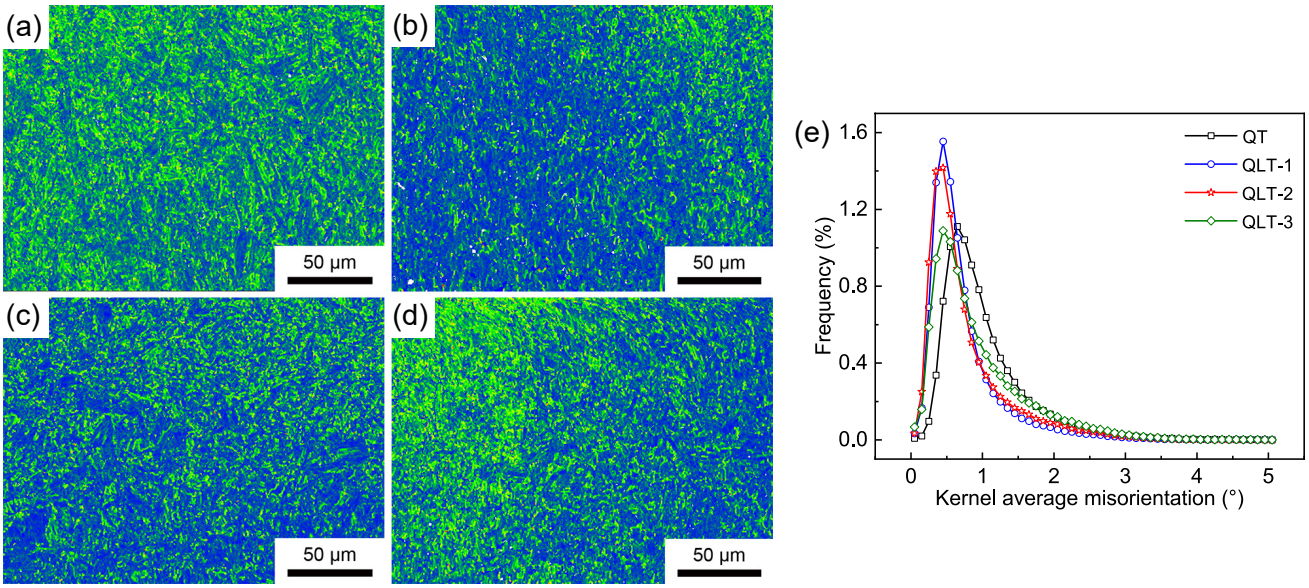

Fig. 11: KAM maps of samples with different heat treatments: (a) QT sample; (b) QLT-1 sample; (c) QLT-2 sample; (d) QLT-3 sample; and (e) KAM distribution

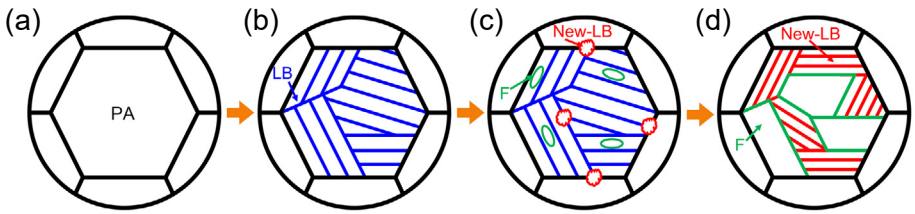

Fig. 12: Schematic diagram of structural transformation

transformation into ferrite (F) [Fig. 12(c)]. Moreover, during the subsequent quenching process, new lath bainite (New-LB) is formed. Ultimately, a dual-phase microstructure consisting of ferrite and new lath bainite is achieved, exhibiting a significantly refined grain size [Fig. 12(d)].

5 Conclusions

This study presents a quenching, lamellarizing, and tempering (QLT) heat treatment method for ZG14Ni3Cr1MoV steel, which results in a dual-phase microstructure with remarkable impact toughness. The microstructure and mechanical properties of the steel were characterized and compared with those of samples treated by conventional quenching and tempering (QT) heat treatment. The key conclusions are as follows:

(1) A dual-phase microstructure consisting of soft ferrite and hard tempered bainite can be obtained through the process of quenching, lamellarizing, and tempering heat treatment. The average grain sizes of the QLT samples lamellarizing at 750 °C, 780 °C, and 810 °C are 45.62 μm, 38.87 μm, and 46.51 μm, respectively, which are significantly finer than the 64.93 μm observed in the QT sample.

(2) With an increase in the lamellar quenching temperature, both the yield strength and tensile strength of the QLT sample increase; however, these values still lower than those of the QT sample. Conversely, the elongation at fracture, reduction of area, and the production of strength and elongation of the QLT sample exhibit a downward trend with rising lamellar quenching temperatures, although they are still higher than those of the QT sample.

(3) The impact absorption energy of the QLT samples within the temperature range of −80 °C to −120 °C is significantly higher than that of the QT samples. After lamellar quenching at 780 °C, the optimal cryogenic toughness is achieved, measuring 215.97 J at −80 °C, 207.80 J at −100 °C, and 183.17 J at −120 °C. The outstanding cryogenic toughness exhibited by the QLT samples can be primarily attributed to two key factors within the dual-phase microstructure. Firstly, the low dislocation density in this microstructure reduces the likelihood of crack initiation. Secondly, the soft ferrite phase effectively passivates the crack tip, while high-angle grain boundaries (HAGBs) act to deflect or hinder crack propagation.

Acknowledgment

This work was financially supported by the Science and Technology Planning Joint Program of Liaoning Province (Applied Basic Research Project, No. 2023JH2/101700054).

Conflict of interest

The authors declare that they have no known competing financial interests or personal relationships that could have appeared to influence the work reported in this paper.

References

[1] Liu D, Cheng B, Chen Y. Strengthening and toughening of a heavy plate steel for shipbuilding with yield strength of approximately 690 MPa. Metallurgical and Materials Transactions: A, 2013, 44(1): 440–455.
[2] Sohrabi M J, Mirzadeh H, Mehranpour M S, et al. Aging kinetics and mechanical properties of copper-bearing low-carbon HSLA-100 microalloyed steel. Archives of Civil and Mechanical Engineering, 2019, 19(4): 1409–1418.
[3] Vervynckt S, Verbeken K, Lopez B, et al. Modern HSLA steels and role of non-recrystallisation temperature. International Materials Reviews, 2012, 57(4): 187–207.
[4] Zhao S Y, Chen K X, Wuqikun Y, et al. Effect of heat treatment on microstructure and mechanical properties of high strength low alloy (HSLA) steel. Research and Application of Materials Science, 2019, 1(2): 31–38.
[5] Kalantar M, Najafi H, Afshar M R. Comparison between vanadium and niobium effects on the mechanical properties of intercritically heat treated microalloyed cast steels. Metals and Materials International, 2019, 25(1): 229–237.
[6] Xie Z J, Han G, Zhou W H, et al. A novel multi-step intercritical heat treatment induces multi-phase microstructure with ultra-low yield ratio and high ductility in advanced high-strength steel. Scripta Materialia, 2018, 155: 164–168.
[7] Xiong X, Yang F, Zou X, et al. Effect of twice quenching and tempering on the mechanical properties and microstructures of SCRAM steel for fusion application. Journal of Nuclear Materials, 2012, 430(1–3): 114–118.
[8] Shafiei E, Heydarian M, Ostovan F, et al. Effect of double quenching-tempering on microstructure and mechanical properties of HSLA-100. Metallography, Microstructure, and Analysis, 2021, 10(6): 768–775.
[9] Yu Y, Hu B, Gao M, et al. Determining role of heterogeneous microstructure in lowering yield ratio and enhancing impact toughness in high-strength low-alloy steel. International Journal of Minerals, Metallurgy and Materials, 2021, 28(5): 816–825.
[10] Wang Z H, Yang C F, Niu J C, et al. Effect of two-phase region heat treatment on cryogenic toughness of ZG14Ni3CrMoV cast steel. Development and Application of Materials, 2017, 32(4): 5–8. (In Chinese)
[11] Nakada N, Fukagawa R, Tsuchiyama T, et al. Inheritance of dislocations and crystallographic texture during martensitic reversion into austenite. ISIJ International, 2013, 53(7): 1286–1288.
[12] Lu J, Yu H, Yang S. Mechanical behavior of multi-stage heat-treated HSLA steel based on examinations of microstructural evolution. Materials Science & Engineering: A, 2021, 803: 140493.
[13] Mani E, Udhayakumar T. Effect of prior austenitic grain size and tempering temperature on the energy absorption characteristics of low alloy quenched and tempered steels. Materials Science & Engineering: A, 2018, 716: 92–98.
[14] Yuan Q, Xiong L, Liang W, et al. Experimental study on single value fluctuation of impact work in 700 MPa low-alloy tempering plate. Journal of Materials Research and Technology, 2024, 32: 565–576.
[15] Wang M, Wu Z, He J, et al. Microstructure and mechanical properties of a cast TRIP-assisted multiphase stainless steel. China Foundry, 2024, 21(3): 221–228.
[16] Cai M H, Ding H, Zhang J S, et al. Deformation and fracture characteristics of ferrite/bainite dual-phase steels. Chinese Journal of Materials Research, 2009, 23(1): 83–88.
[17] Lee C G, Kim S J, Lee T H, et al. Effects of volume fraction and stability of retained austenite on formability in a 0.1C-1.5Si-1.5Mn-0.5Cu TRIP-aided cold-rolled steel sheet. Materials Science and Engineering: A, 2004, 371(1–2): 16–23.
[18] Zhang W X, Chen Y Z, Cong Y B, et al. On the austenite stability of cryogenic Ni steels: microstructural effects: A review. Journal of Materials Science, 2021, 56(22): 12539–12558.
[19] Dolzhenko A, Belyakov A, Kaibyshev R. Effect of tempforming temperature on the impact toughness of an HSLA steel. ISIJ International, 2023, 63(2): 382–389.
[20] Izumiyama Y, Kayano R, Nagai K. Ductile-to-brittle transition in a quenched and tempered low carbon high strength steel with intermediate stage transformation microstructures. Tetsu to Hagane-Journal of the Iron and Steel Institute of Japan, 2014, 100(5): 112–120.
[21] Inoue T, Yin F, Kimura Y, et al. Delamination effect on impact properties of ultrafine-grained low-carbon steel processed by warm caliber rolling. Metallurgical and Materials Transactions: A, 2010, 41(2): 341–355.
[22] Morris Jr J W. Stronger, tougher steels. Science, 2008, 320(5879): 1022–1023.
[23] Han J, Da Silva A K, Ponge D, et al. The effects of prior austenite grain boundaries and microstructural morphology on the impact toughness of intercritically annealed medium Mn steel. Acta Materialia, 2017, 122: 199–206.
[24] Sk M B, Alam I, Chakrabarti D. The role of fibrous morphology on the Charpy impact properties of low carbon ferrite-bainite dual phase steel. Materials Science & Engineering: A, 2018, 716: 208–219.
[25] Isasti N, Jorge-Badiola D, Taheri M L, et al. Effect of composition and deformation on coarse-grained austenite transformation in Nb-Mo microalloyed steels. Metallurgical and Materials Transactions: A, 2011, 42(12): 3729–3742.
[26] He B B, Hu B, Yen H W, et al. High dislocation density-induced large ductility in deformed and partitioned steels. Science, 2017, 357(6355): 1029–1032.
[27] Yong Q L. Secondary phases in steels. Beijing: Metallurgical Industry Press, 2006. (In Chinese)